Resolved Resonance Evaluation for Neutron Interactions with 103 Rh Up to 8 keV

Luiz Leal, Nicolas Leclaire, Frédéric Fernex, Devin Barry, Peter Schillebeeckx, Stefan Kopecky

Nuclear Science and Engineering

ISSN: (Print) (Online) Journal homepage: www.tandfonline.com/journals/unse20

Resolved Resonance Evaluation for Neutron Interactions with ^{103}Rh Up to 8 keV

Luiz Leal, Nicolas Leclaire, Frédéric Fernex, Devin Barry, Peter Schillebeeckx & Stefan Kopecky

To cite this article: Luiz Leal, Nicolas Leclaire, Frédéric Fernex, Devin Barry, Peter Schillebeeckx & Stefan Kopecky (04 Nov 2024): Resolved Resonance Evaluation for Neutron Interactions with ^{103}Rh Up to 8 keV, Nuclear Science and Engineering, DOI: 10.1080/00295639.2024.2411171

To link to this article: https://doi.org/10.1080/00295639.2024.2411171

Published online: 04 Nov 2024.

NUCLEAR SCIENCE AND ENGINEERING

DOI: https://doi.org/10.1080/00295639.2024.2411171

Resolved Resonance Evaluation for Neutron Interactions with ^{103}Rh Up to 8 keV

Luiz Leal,[a]* Nicolas Leclaire,[b] Frédéric Fernex,[b] Devin Barry,[c] Peter Schillebeeckx,[d] and Stefan Kopecky[d]

[a]*Oak Ridge National Laboratory, Nuclear Energy and Fuel Cycle Division, Oak Ridge, Tennessee*
[b]*Institut de Radioprotection et de Sûreté Nucléaire, 31 avenue de la division Leclerc, Fontenay-aux-Roses, 92260, France*
[c]*Naval Nuclear Laboratory, P.O. Box 1072, Schenectady, New York 12301-1072*
[d]*EC, JRC-Geel, Retieseweg 111, B-2440, Geel, Belgium*

Received May 13, 2024
Accepted for Publication September 21, 2024

Abstract — *A neutron cross-section evaluation for the n + ^{103}Rh reaction in the resolved resonance region was carried out in the energy range 10^{-5} eV to 8 keV encompassing thermal energy at 0.0253 eV. The scope of this work is to generate resonance parameters and resonance parameter covariances based on the Reich-Moore reduced R-matrix formalism using the code SAMMY. Some features of the new evaluation are the inclusion of high-resolution capture data in the SAMMY evaluation process and the extension of the resolved resonance range from 4 to 8 keV. Furthermore, the evaluation employs more accurate resonance parameter representation by exploring the use of the LRF = 7 ENDF feature and also the use of the LCOMP = 2 compact format for resonance parameter covariance representation. Included in the SAMMY evaluation are transmission data, capture cross-section data, and neutron scattering length information. Thermal cross-section values listed in the literature, as well as capture resonance integrals, were also incorporated into the evaluation process.*

Keywords — *Nuclear data, uncertainty, differential and integral data, data evaluation.*

Note — *Some figures may be in color only in the electronic version.*

I. INTRODUCTION

As a nuclear reactor operates, the stable isotope ^{103}Rh is produced as a fission product. Indeed, no ^{103}Rh is present at the reactor's start of operation. The only naturally occurring rhodium isotope is ^{103}Rh. Rhodium is also used as part of neutron flux detectors in nuclear reactors. It is an important fission-product absorber that can decrease reactor reactivity and that can be encountered in nuclear criticality safety applications outside reactors. The accumulation of fission products in spent nuclear fuel is responsible for a decrease in reactivity, known as burnup credit, which can lead to cost savings in packaging, transport, and storage of spent nuclear fuel. Therefore, accurate knowledge of the cross sections of fission products and their uncertainties is important, in particular for ^{103}Rh given its importance as a fission product.[1]

A ^{103}Rh resonance evaluation was done in the energy range from 10^{-5} eV to 8 keV using the Reich-Moore reduced R-matrix formalism of the SAMMY code.[2] Compared with resonance evaluations included

*E-mail: lealIc@ornl.gov

in the existing nuclear data library,[3] the present evaluation extends the resonance region from 4 to 8 keV. The evaluation took advantage of the LRF = 7 resonance parameter ENDF representation,[4] which is often referred to as the R-matrix limited format. The main feature of this format is that it allows for the use of detailed information on resonance spin to account for interference effects. This information is needed for a good reproduction of the cross sections on the basis of a resonance representation.

Isotope ^{103}Rh is an odd-even isotope with ground-state spin and a parity of $I = 1/2^-$. The half-integer ground-state spin leads to two possible channel spins for the $n + {}^{103}$Rh reaction, given that the neutron spin and parity is $i = 1/2^+$. The channel spins and parities are $s = 0^-$ and $s = 1^-$, respectively. The spin-parity combinations for the $n + {}^{103}$Rh reaction, for $l = 0$ (s-wave) and $l = 1$ (p-wave), are displayed in Table I. Resonance interference effects are properly described by using the correct spin-channel representation in the SAMMY evaluation process.

This paper presents the resonance analysis results of several transmission and capture data in the energy range of 10^{-5} eV to 8 keV. Resonance integral, cross section at energy 0.0253 eV (thermal), and neutron scattering length data were also included in the evaluation. The statistical properties of the parameters were examined, and resonance parameter covariance (RPC) was generated. Benchmark testing of the evaluation was carried out, and the effect of the uncertainty on the multiplication factor due to the RPC was investigated.

The following sections describe the strategy used to evaluate the experimental data. Later sections are devoted to examining the statistical properties of the resonance parameters. The effect of the new evaluation on integral benchmark calculations is also presented. The calculated thermal cross section, resonance integral, and coherent scattering length are compared with existing experimental data. Uncertainties owing to the RPC generated in the evaluation are propagated to the calculated values.

TABLE I

$n + {}^{103}$Rh Spin and Parity for s- and p-Waves

l	s	J
0	0^-	0^-
	1^-	1^-
1	0^-	1^+
	1^-	$0^+, 1^+, 2^+$

II. EXPERIMENTAL DATA

A comprehensive examination of the ^{103}Rh experimental data available in EXFOR[5] was done. The criteria for selecting the ^{103}Rh experimental data were mainly based on the available experimental information, such as, for example, the experimental data resolution. In addition, one important aspect of this work was the extension of the resonance region up to 8 keV. Very few experimental data with good resolution exist in EXFOR above 4 keV that could be used in the evaluation. The majority of the experimental data used in the evaluation were from measurements performed at the Geel Electron Linear Accelerator (GELINA) in Belgium[6] and from the Gaerttner Linear Accelerator (LINAC) facility at the Rensselaer Polytechnic Institute (RPI)[7] in Troy, New York.

This paper relies heavily on data from RPI and GELINA, given the easy accessibility to the data and the information about the experimental conditions. The GELINA experimental data used in the evaluation are listed in Table II, which includes the references to the data, energy ranges, areal number density of the samples, and flight path length. The RPI experimental data used in the evaluation were obtained via personal communication.[8] The RPI experimental data are displayed in Table III.

A brief description of the analysis and evaluation of the GELINA experimental data is provided elsewhere.[9] An additional description is included in this paper. In addition to the time-of-flight data, the evaluation also included information such as coherent scattering length, capture Wescott factor, and capture resonance integral.

III. RESONANCE PARAMETER EVALUATION

This section is dedicated to describing the procedure used to evaluate the ^{103}Rh resonance up to 8 keV. The resonance parameters and RPC for ^{103}Rh were determined by a self-consistent analysis of several experimental data sets introduced in the previous section. The R-matrix code SAMMY was used for the analysis. SAMMY incorporates Doppler and resolution broadening, as well as other experimental effects, such as multiple-scattering effects.

The analysis started from a set of resonance parameters available in the existing evaluated data file ENDF/B-VIII.0,[3] which uses a multilevel Breit-Wigner approximation of the R-matrix formalism. The ENDF/B-VIII.0

TABLE II

GELINA Experimental Data

Reference	Energy Range (eV)	Data
Transmission		
Brusegan et al.[16]	0.4 to 1000	49.3 m, 0.002207 at/b
Brusegan et al.[16]	0.4 to 1000	49.3 m, 0.000337 at/b
Ribon[14]	18.0 to 95.0	53.7 m, 0.00608 at/b
Ribon[14]	84.0 to 503.0	53.7 m, 0.0001487 at/b
Ribon[14]	178.0 to 757.0	53.7 m, 0.05 at/b
Ribon[14]	600.0 to 4000	103.7 m, 0.02435 at/b
Mihailescu et al.[10]	1.85 to 8000	49.343 m, 0.0458 at/b
Capture		
Brusegan et al.[16]	0.01 to 1000	14.3624 m, 0.00187 at/b
Mihailescu et al.[10]	1.72 to 8000	28.814 m, 0.000337 at/b
Mihailescu et al.[10]	1.72 to 8000	28.814 m, 0.00187 at/b

TABLE III

RPI LINAC Experimental Data

Reference	Energy Range (eV)	Data
Transmission		
Barry[8]	0.01 to 10	14.973 m, 0.0003505 at/b
	0.01 to 10	14.973 m, 0.000743 at/b
	0.01 to 10	14.973 m, 0.003790 at/b
	0.01 to 10	14.973 m, 0.00944 at/b
	0.01 to 10	14.973 m, 0.01882 at/b
	0.5 to 2000	25.589 m, 0.001925 at/b
	0.5 to 2000	25.589 m, 0.003790 at/b
	0.5 to 2000	25.589 m, 0.00944 at/b
	0.5 to 2000	25.589 m, 0.01882 at/b
Capture		
Barry[8]	0.01 to 10	25.444 m, 0.0002006 at/b
	0.01 to 10	25.444 m, 0.0003505 at/b
	0.01 to 10	25.444 m, 0.000743 at/b
	0.01 to 10	25.444 m, 0.001925 at/b
	0.01 to 10	25.444 m, 0.003790 at/b
	0.6 to 560	25.564 m, 0.0002006 at/b
	0.6 to 560	25.564 m, 0.0003505 at/b
	0.6 to 560	25.564 m, 0.000743 at/b
	0.6 to 560	25.564 m, 0.001925 at/b
	0.6 to 560	25.564 m, 0.003790 at/b
	0.6 to 560	25.564 m, 0.00944 at/b
	0.6 to 560	25.564 m, 0.01882 at/b

^{103}Rh resonance parameters are available up to 4170 eV. One of the main issues with the ENDF/B-VIII evaluation is that the resonance spin channel for the n + ^{103}Rh reaction was not properly described. The evaluation may have been completed before the ENDF-6[4] format was updated. The ENDF-6 format update allows for

a more comprehensive representation of the reaction spin distribution.

The new evaluation has the following features:

1. Extends the resonance region up to 8000 eV.
2. Includes the correct channel spin representation.
3. Generates resonance parameters using the LRF = 7.
4. Generates RPC using the compact formalism (i.e., LCOMP = 2).
5. Includes neutron scattering length information.

The available experimental data that permitted the resonance region extension from 4000 to 8000 eV were those of Mihailescu et al.[10] Because no resonance parameters existed above 4000 eV, a peak search similar to that of Sayer[11] using the Mihailescu et al. transmission data was carried out to determine the resonance energies. Neutron capture widths were taken as the average of those values below 4000 eV and used as the prior before the SAMMY fit of the data.

The peak search also provided an initial guess for the neutron resonance width. The angular momentum l contributing to the total angular momentum J of the resonances was examined according to the energy dependence of the penetrability factor $P_l(E)$. The energy dependence of the neutron centrifugal barrier penetration factor is given by

$$V_l(E) = P_l(E)/\rho \quad , \tag{1}$$

where $\rho = ka$, k is the wave number, and a is the channel radius.

The plot in Fig. 1 clearly shows that $l = 0$ and $l = 1$ (i.e., the s- and p-waves) contribute the most in the energy range up to 8000 keV. Random sets of resonance spins were generated and used to fit the data. According to Table I, six spin groups were used for the resonance spin sampling. For some of the resonances, an estimate based on knowledge and experience was used to assign resonance spins. The following strategy was used to assign spins:

1. In the energy range above 4000 keV, 100 sets of resonance spins were randomly generated.
2. The code SAMMY was run 100 times for fitting Mihailescu et al. capture and transmission data.
3. The results with the best χ^2 value were retained.

Although the procedure seemed demanding, it worked quite well. The next step involved determining

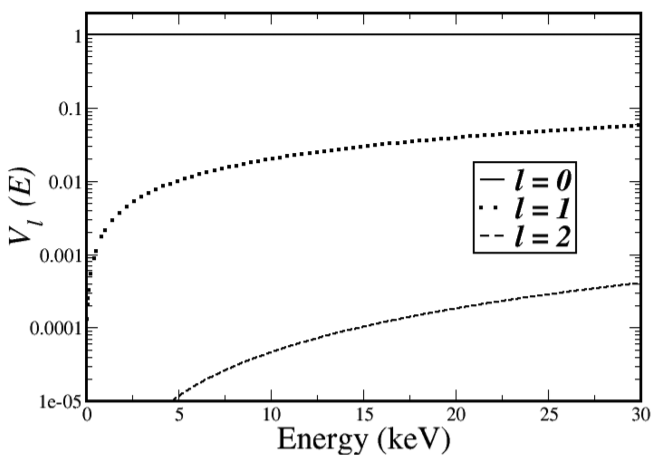

Fig. 1. Energy dependence of the neutron centrifugal penetration factor $V_l(E)$ for ^{103}Rh.

the resonance parameter contribution owing to the external energy levels; that is, negative bound levels and energy levels above 8000 keV. The methodology used is described elsewhere.[12] These external resonances contribute to the scattering cross-section energy dependence. Six energy levels were determined: three negative bound levels and three energy levels above 8000 keV. The negative energy levels close to zero were adjusted to fit thermal cross sections and coherent scattering lengths.

Other alternatives, such as that by Fröhner and Bouland[13], can also be used to determine the external energy level. The external level contribution to the scattering cross section is shown in Fig. 2. Also shown in Fig. 2 is the contribution of the external energy levels based on ENDF/B-VIII.0[3] resonance parameters (in red) up to 4000 eV and the new resonance parameters derived in

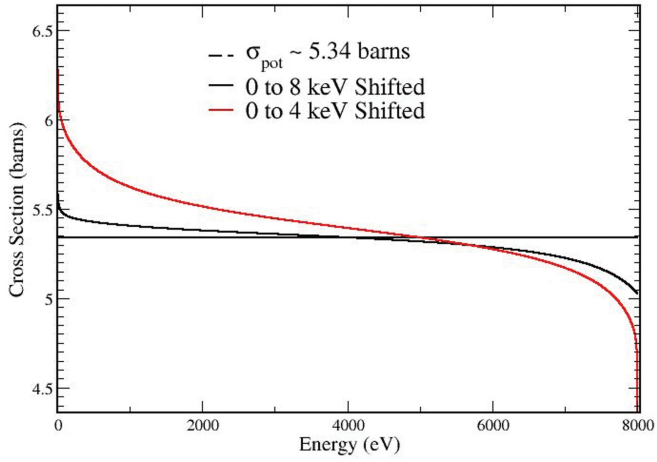

Fig. 2. External level contribution to the scattering cross section. The result in red was obtained using ENDF/B-VIII.0 resonance parameters up 4000 eV.

this evaluation (in black). Clearly, the new evaluation provides an energy dependence of the external level symmetric around 4000 eV. A suitable determination of the contribution of the external resonance leads to an accurate determination of the effective scattering radius, and consequently, a good fit of the transmission data (total cross section).

III.A. Experimental Data Normalization and Background

Consistency between the experimental data used in the evaluation can only be achieved by seeking normalization and background corrections in connection with the experimental data. The SAMMY code was used to search for the normalization and background corrections suitable to the experimental data. The effects of the neutron background cross section on a time-of-flight measurement are generally represented as a constant background related to the environment and time-dependent in connection with neutrons scattered throughout the detector.

The latter can be considered as a $1/\sqrt{E}$ cross section, based on the $1/v$ cross-section behavior. This is an approximation, and in reality, the time-dependent background can be more complicated. Few functional forms are available in the code SAMMY to account for the background corrections. The following equation was used in this work:

$$a + \frac{b}{\sqrt{E}}\,, \tag{2}$$

where a and b are constants with a dimensionless and b given in units of $\sqrt{\text{eV}}$. The SAMMY search for a and b for the GELINA experimental data are reported in Table IV. The normalization for the Ribon[14] data listed in Table II ranged from 0.92 to 1.08. Similar searches for normalization and background corrections were carried out for the RPI data. Normalization and background corrections for the RPI transmission and capture data are listed in Table V. Tables IV and V indicate the consistency of the GELINA and RPI data. In the thermal energy range, Lee et al. capture data[15] indicated a normalization of about 8% for consistency with the Brusegan et al. capture data.[16]

III.B. Thermal Energy Range

Five transmission and five capture yield data with distinct thicknesses from the RPI LINAC facility[8] were used in the energy range from 0.01 to 10 eV. Capture data from Brusegan et al.[16] and Lee et al.[15] were also used, along with the total cross sections of Havens and Rainwater[17] and Sailor.[18] Fitting of the RPI capture yield data and transmission data are displayed in Figs. 3 and 4, respectively. The capture data fitting results of Brusegan et al.[16] and Lee et al.[15] are shown in Fig. 5, and the total cross section of Havens and Rainwater[17] and Sailor[18] are shown in Fig. 6.

Comparisons of the capture cross section at thermal (0.0253 eV) with experimental values from Brusegan et al.[16] and Lee et al.[15] are shown in Table VI. The thermal values obtained in the measurements done by Lee et al.[15] seem too low. The numbers in parentheses in Table VI indicate uncertainty at a 68% confidence interval, or one standard deviation.

TABLE IV

Normalization and Background Correction for GELINA Data

	Normalization	Background Correction
Transmission		
Experimental data	n	a, b ($\sqrt{\text{eV}}$)
Brusegan et al.[16]	1.0032	-2.60×10^{-3}, -2.90×10^{-3}
Brusegan et al.[16]	0.9842	3.69×10^{-2}, -9.00×10^{-4}
Mihailescu et al.[10]	0.9814	1.11×10^{-2}, -5.09×10^{-2}
Capture		
Brusegan et al.[16]	1.0090	6.00×10^{-4}, -4.00×10^{-4}
Mihailescu et al.[10]	0.9617	-4.00×10^{-5}, 1.10×10^{-3}
Mihailescu et al.[10]	0.9899	-8.48×10^{-5}, 3.40×10^{-3}

TABLE V

Normalization and Background Correction for RPI Data

	Normalization	Background Correction
Transmission		
Areal number density data (at/b)	n	a, b ($\sqrt{\text{eV}}$)
0.0019249	0.9992	2.00×10^{-4}, 1.00×10^{-4}
0.0037901	0.9981	1.00×10^{-4}, 2.00×10^{-4}
0.0094397	0.9966	3.00×10^{-4}, 1.00×10^{-4}
0.018816	0.9948	2.00×10^{-4}, 2.00×10^{-4}
Capture		
0.0002006	1.0448	-6.05×10^{-5}, 1.00×10^{-4}
0.0003505	0.9878	-7.05×10^{-5}, 2.00×10^{-4}
0.0007427	1.0119	-8.77×10^{-5}, 2.20×10^{-4}
0.0019249	0.9988	-9.19×10^{-5}, -1.32×10^{-5}
0.0037901	0.9949	-6.24×10^{-5}, 1.00×10^{-4}

The uncertainties in the results presented in Table VI, and throughout this paper, follow the rules indicated in Ref. [19]. The thermal values listed in existing cross-section libraries, namely, ENDF/B-VIII.0[3] and JEFF3.3,[20] as well as the values listed in the *Atlas of Neutron Resonances*,[21] are shown in Table VII. Also shown in Table VII is the resonance capture integral. The values obtained in this work are in good agreement with the values listed in the *Atlas*. Other quantities calculated using the new evaluations were the capture Westcott's g-factor, which was 1.024, and a Maxwellian average of capture cross sections of 129.64 barn for kT = 0.0253 eV.

III.C. Neutron Scattering Length Information

Coherent and incoherent scattering length information were added to the evaluation process. This information helped determine the bound levels and scattering cross section. Spin-dependent coherent and incoherent

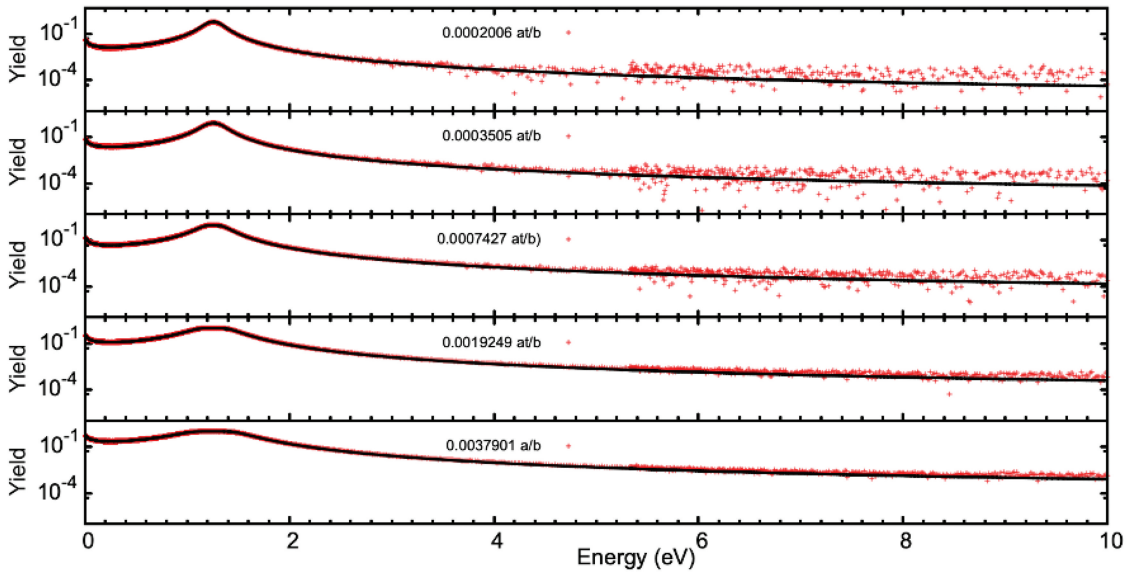

Fig. 3. SAMMY fitting of the RPI capture data.

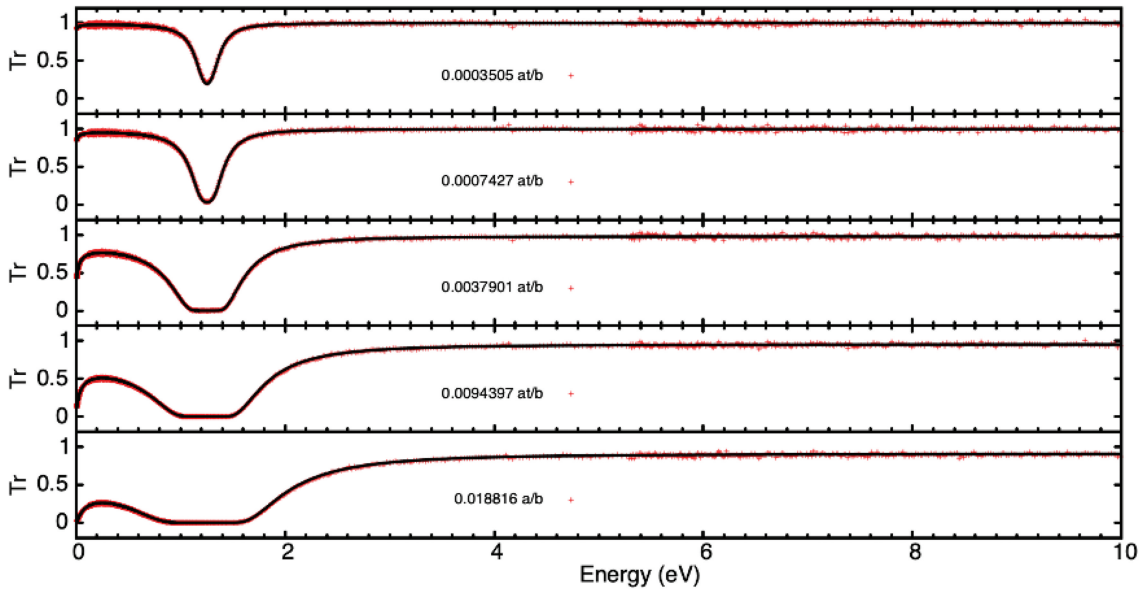

Fig. 4. SAMMY fitting of the RPI transmission data.

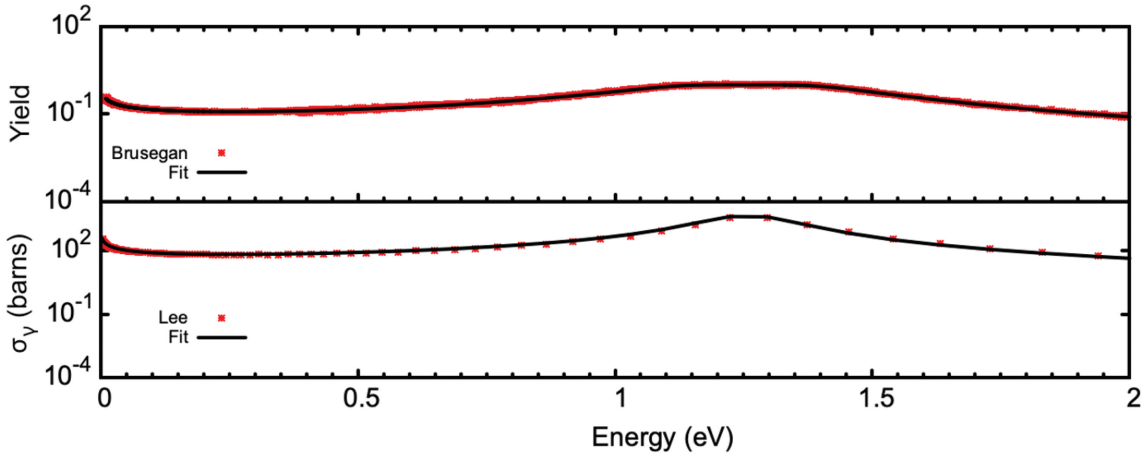

Fig. 5. SAMMY fitting of the Brusegan et al. and Lee et al. capture data below 2 eV.

scattering lengths were determined according to the following equations[22]:

$$a_{\text{coh}} = \frac{I+1}{2I+1}a^{+} + \frac{I}{2I+1}a^{-} \tag{3}$$

$$a_{\text{incoh}} = \frac{[I(I+1)]^{1/2}}{2I+1}(a^{+} - a^{-}) \quad , \tag{4}$$

where I is the target spin, and a^{-} and a^{+} are the s-wave scattering lengths determined for the total angular spin $J^{\pi} = 0^{-}$ and 1^{-}, respectively. The values for a^{-} and a^{+} were calculated using SAMMY from the scattering cross sections $\sigma_s(0^{-})$ and $\sigma_s(1^{-})$, which were obtained via the resonance parameters. Note that $\sigma_s(J^{\pi})$ is the portion of the scattering cross section corresponding to the total angular momentum J^{π}. The unbounded values calculated using the resonance parameters for $T = 0$ K are displayed in Table VIII.

This evaluation used the initial values for the unbounded coherent and incoherent scattering lengths available in the literature[23]: 5.84 (4) fm and 0.60 (4) fm, respectively. The evaluated coherent scattering value agreed with the value listed in the literature, but the incoherent scattering was far from the initial values. This difference is not well understood. It is worth mentioning that there are discrepancies outside this work as to the scattering length values, mainly for the incoherent scattering cross sections of ^{103}Rh.

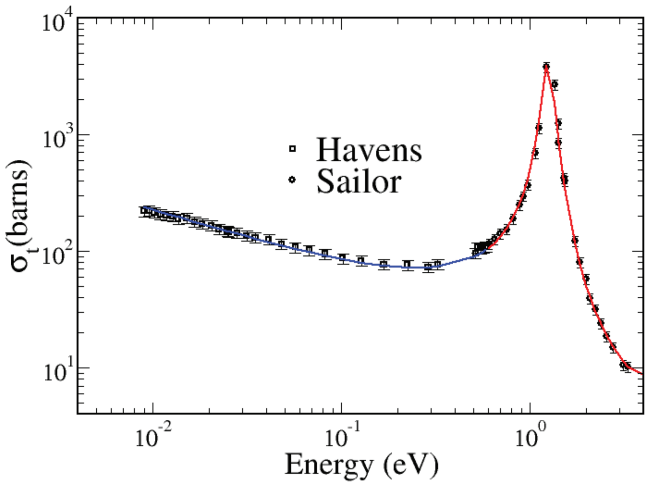

Fig. 6. SAMMY fitting of the Havens and Rainwater[17] and Sailor[18] total cross section below 3 eV.

TABLE VI

Capture Cross Section at Thermal and 296.3 K*

Brusegan et al.[16]	142.5 (15)
Lee et al.[15]	133.00 (93)
This work	142.8 (23)

*Capture cross section in barns and thermal at 0.0253 eV.

TABLE VII

Thermal Capture and Resonance Integral

Evaluation	$\sigma_\gamma\,(b)$	$I_\gamma\,(b)$
Atlas[21]	143.5 (15)	1012 (50)
ENDF/B-VIII.0[3]	142.1	968
JEFF3.3[20]	142.8	969
This work	142.8 (23)	1007 (41)

The bound values were obtained by multiplying the results in Table VIII by $(A+1)/A$, where A is the atomic mass relative to the mass of a neutron, which is 102.021 for ^{103}Rh.

III.D. The ^{103}Rh Resonance Evaluation Up to 8000 eV

In the energy region up to 8000 eV, the SAMMY analysis of the experimental data presented previously identified 549 resonances, namely, 197 *s*-waves and 352 *p*-waves. The first resonance in the $n + {}^{103}$Rh reaction is a *s*-wave located at the resonance energy $E_r = 1.259$ eV, with total angular momentum and parity of $J = 1^-$. The fitting of the experimental data below 5 eV, including the thermal energy, were shown in Sec. III.B.

An excellent fit of the experimental data with the SAMMY code was obtained for all experimental data up to 8000 eV. As an example, the fit of the Mihailescu et al.[10] transmission data from 1.85 to 8000 eV is displayed in Fig. 7 together with residues. Likewise, Figs. 8 and 9 display the fit of the RPI transmission and capture cross section and residues, respectively, in the energy range from 100 to 500 eV. The residues were calculated as $(T-E)/\delta E$, where T represents the theory, E the experiment, and δE the uncertainty in the experimental data. The Bayesian χ^2 for the experimental data fitting with the SAMMY code ranged from 0.95 to 1.3.

III.D.1. Fitting of the RPI Experimental Data

Five transmission data and five capture yield data were fitted with SAMMY in the energy below 10 eV. The results, which deal with the thermal energy region, are shown in Figs. 3 and 4. In the energy range from 0.6 to 570 eV, five capture yields with thinner samples and two with thicker samples, measured at a flight path of 25.264 m, were analyzed using SAMMY. The results are shown in Figs. 10 and 11. A few spikes, which may be attributed to platinum impurities in the sample, can be observed at energies around 90 eV, 120 eV, and 395 eV.

In the energy range from 0.5 to 2000 eV, four transmission data with different thicknesses were analyzed. The results of the SAMMY fit to the data are shown in Fig. 12. Some spikes can also be observed in the transmission measurements. They are not impurities, but are due to the cadmium fixed-notch filter used

TABLE VIII

Coherent and Incoherent Unbounded Values

a_{coh} (fm)	a_{incoh} (fm)	$\sigma_{coh}(b)$	$\sigma_{incoh}(b)$	$\sigma_s(0^-)(b)$	$\sigma_s(1^-)(b)$
5.72 (4)	0.15 (1)	4.19 (5)	0.28 (1)	2.16 (3)	2.23 (4)

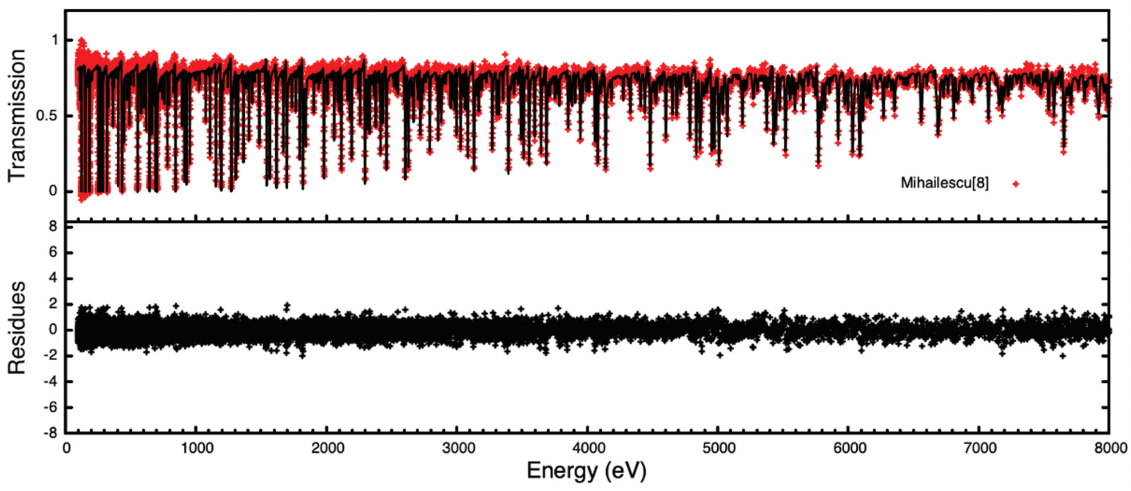

Fig. 7. SAMMY fitting of the Mihailescu et al.[10] transmission data and residues.

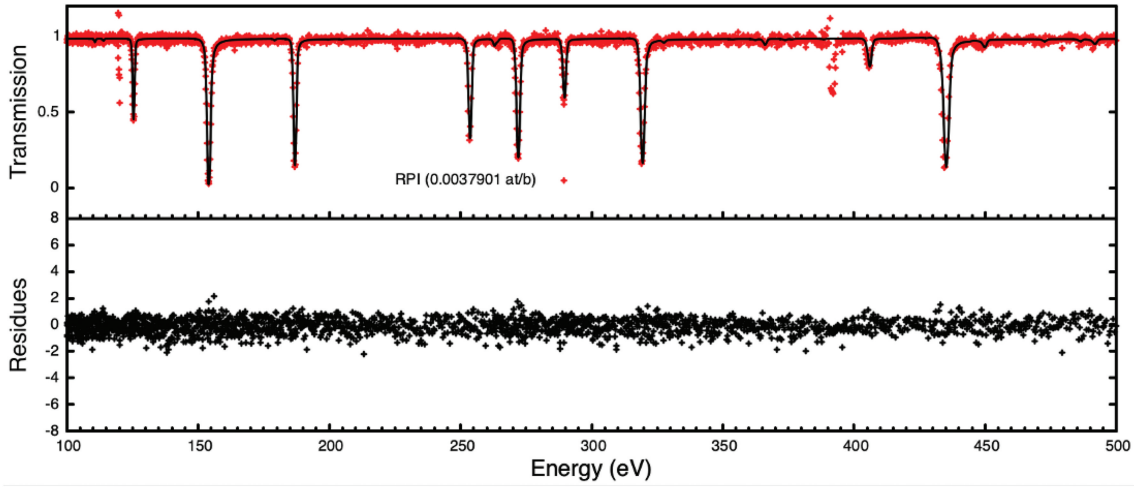

Fig. 8. SAMMY fitting of the RPI transmission data and residues.

during the experiment. Overall, the RPI experimental data were used in the SAMMY fitting in the energy range below 2000 eV. The experimental data were taken at the temperature of 293.6 K. As shown in the Fig. 12, the resonance parameters obtained via the SAMMY fit reproduced the RPI experimental data well.

III.D.2. Fitting of the GELINA Experimental Data

The experimental data from GELINA, shown in Table II, were used in the SAMMY analysis. In particular, the Mihailescu et al.[10] transmission data and capture yield data were crucial in the SAMMY fitting, allowing for the resonance region to extend from 4000 to 8000 eV. The SAMMY fitting of the three Mihailescu et al.[10] data are displayed in Fig. 13. The results for the transmission data are similar to those shown in Fig. 7, in which the residues are also shown.

The transmission data of Ribon[14] measured at a 103.7-m flight path are shown in Fig. 14 together with the Mihailescu et al.[10] transmission data.

The results of the SAMMY fitting of the experimental transmission data and yield data of Brusegan et al.[16] are displayed in Fig. 15. The transmission sample thicknesses were 0.000337 and 0.002207 at/b, respectively, and the capture yield sample thickness was 0.0458 at/b.

III.D.3. Statistical Analysis of Resonance Parameters

Statistical analysis was performed for the ^{103}Rh *s*-wave and *p*-wave resonance parameters derived in this work.

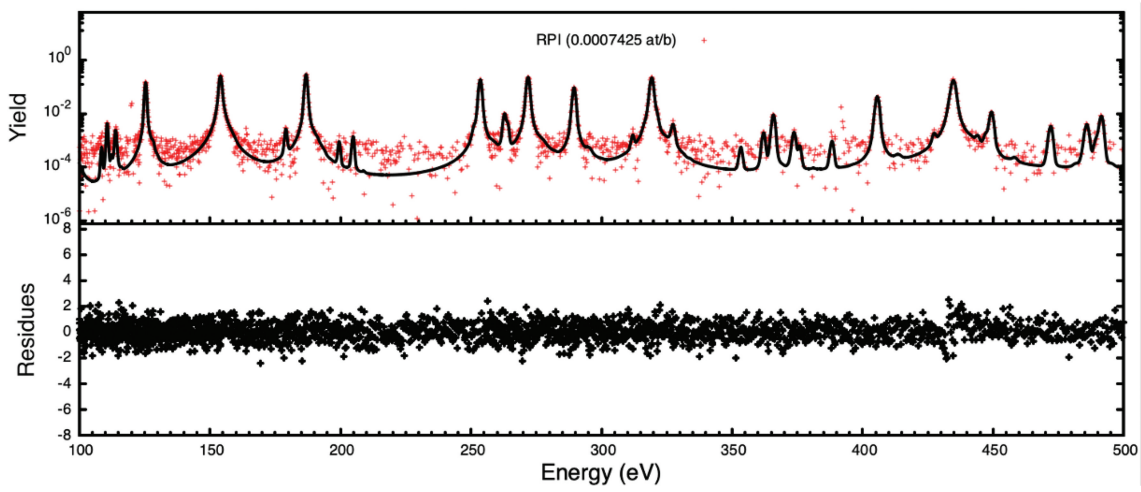

Fig. 9. SAMMY fitting of the RPI capture yield data and residues.

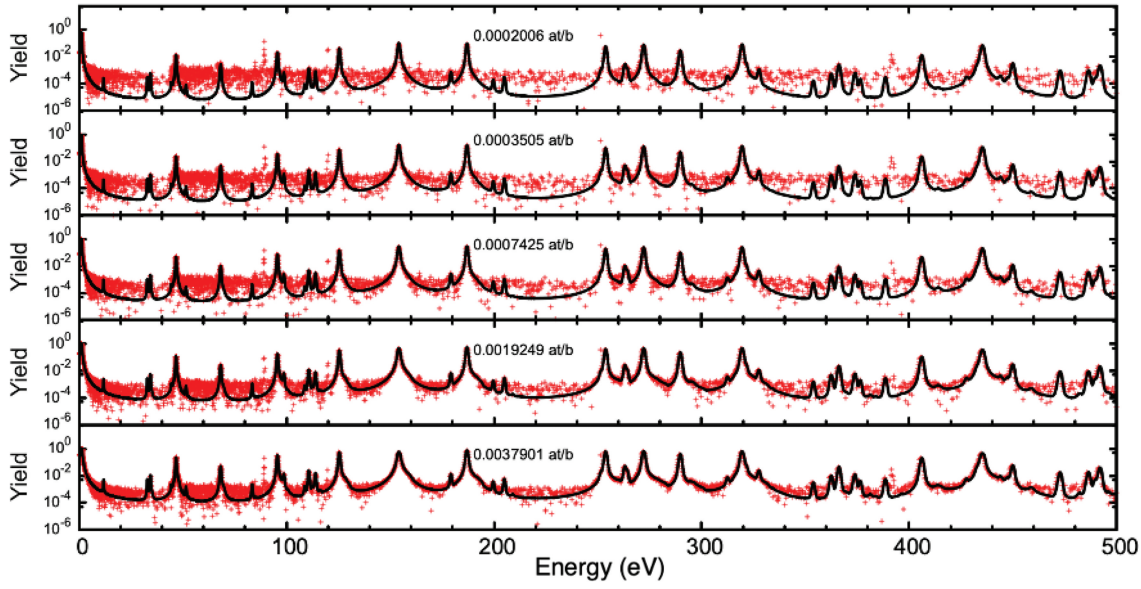

Fig. 10. SAMMY fitting of the RPI capture yield data.

According to Table I, the two total angular momentum and parity J^{π} for the *s*-wave resonances were 0^- and 1^-, respectively. For a level spacing density proportional to $2J+1$, the ratio of the average spacing of the two J total angular momentum was $D^{0^-}/D^{1^-} \approx 1/3$, which indicated that resonances in the spin state 0^- were less frequent than those in the spin state 1^-.

The average level spacing values for each spin in the energy range from thermal to 500 eV are shown in Table IX. The ratio D^{0^-}/D^{1^-} was 0.36, which is in good agreement with the $1/3$ mentioned previously. Also shown in Table IX is the neutron strength function S_{nl}. The average level spacing and the neutron strength function for the mixed spins were 28.89 (38) eV and $10^{4} \times S_{nl} = 0.52$ (10), respectively.

The number of missing *s*-wave resonances, as a function of energy, in four energy ranges, namely, 0 to 500 eV, 0 to 1000 eV, 0 to 4000 eV, and 0 to 8000 eV were determined[24] and are presented in Table X. The measured Δ_3-statistic results, calculated using the SAMDIST code[25] for the *s*-wave resonances up to 500 eV were 0.33, compared with theoretical results of 0.29 (11). Comparisons of the cumulative number of resonances up to 500 eV extended to 8000 eV are shown in Fig. 16. Clearly, the energy resolution affected the identification of small energy resonances. However, the fitting of the experimental data

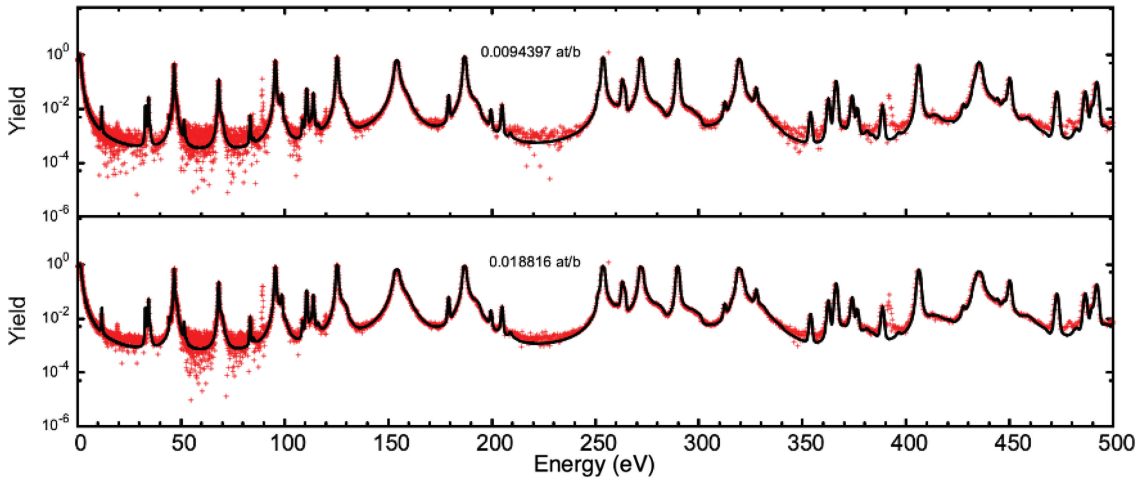

Fig. 11. SAMMY fitting of the RPI capture yield data for thicker samples.

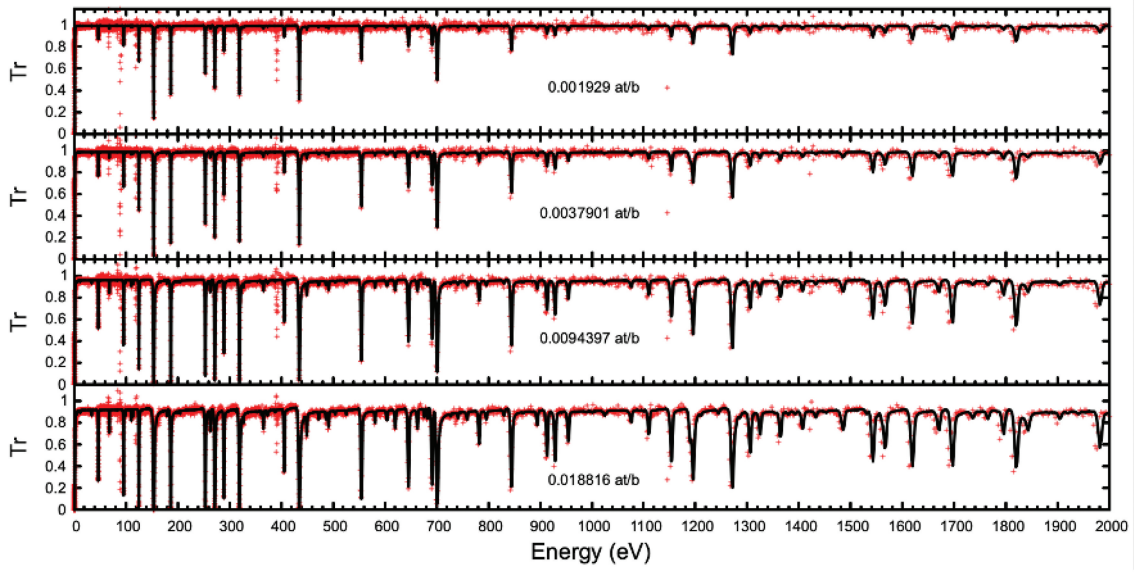

Fig. 12. SAMMY fitting of the RPI transmission data.

was not affected. The average evaluated radiative capture width corresponding to the *s*-wave was 186.24 (412) MeV.

The cumulative Porter-Thomas *s*-wave distributions of the reduced neutron width for the total angular momentum $J = 0^-$, $J = 1^-$, and mixed spin up to 8000 eV are shown in Fig. 17.

The statistical distribution of the *p*-wave resonance parameters was also analyzed. According to Table I, the *p*-wave had three total angular momenta J with spin 0^+, 1^+, and 2^+, respectively, and the spin 1^+ included two input channels, $s = 0^-$ and $s = 1^-$. As mentioned previously, the existing resonance parameter evaluations treated the two spin channels separately, as if the channel spins represented resonances with angular momentum and parity J^π. Consequently, those evaluations did not describe the interference effects correctly. The average spacing for the mixed spins up to 500 eV was $< D > = 15.01\ (273)$ eV, and the wave strength function was $10^{4} \times S_{nl} = 6.81\ (125)$.

III.E. Covariance Generation

The result of a SAMMY evaluation of the experimental data and uncertainty consisted of a parameterization of the neutron cross section in a form $\sigma(p_1, p_2, \ldots, p_n)$, where $p_1, p_2, \ldots, p_n$ are the

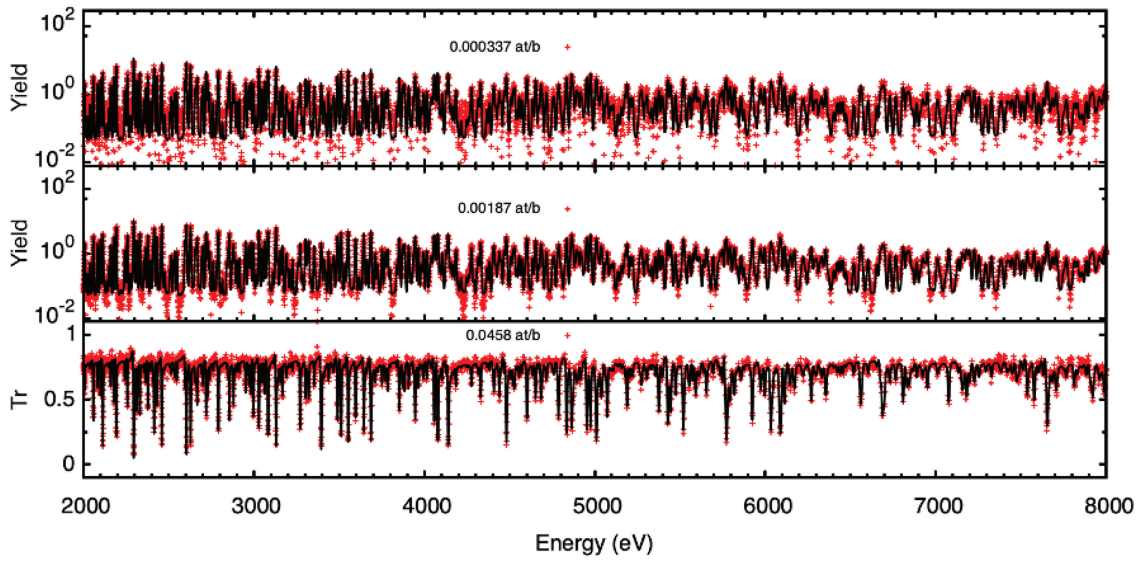

Fig. 13. SAMMY fitting of transmission and capture yield data of Mihailescu et al.[10]

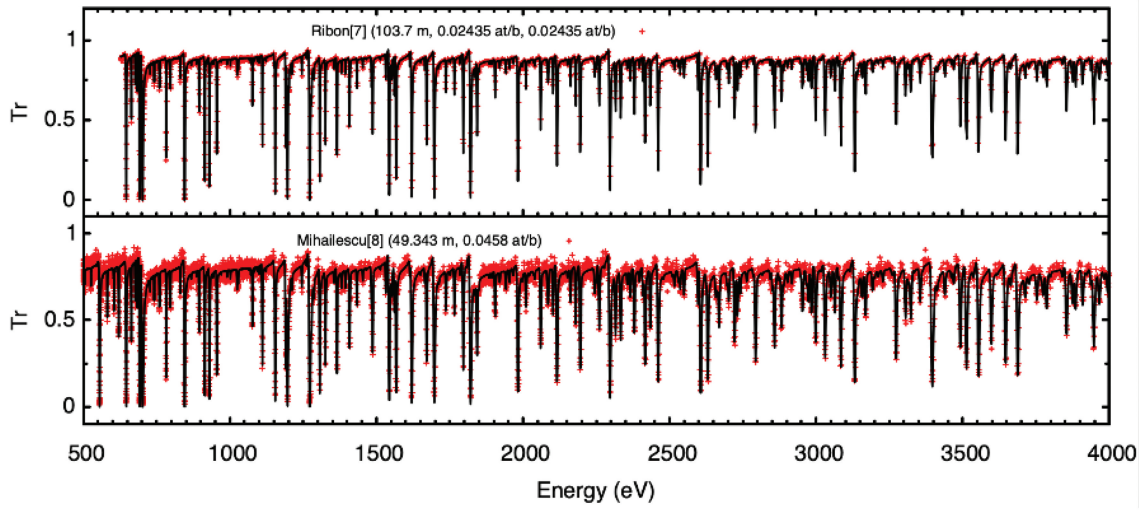

Fig. 14. SAMMY fitting of transmission data of Ribon[14] and Mihailescu et al.[10]

resonance parameters. Furthermore, the cross-section uncertainty was obtained via the RPC and correlations, which in turn were driven by the uncertainty in the experimental data. The sources of experimental uncertainties included in the covariance generation were those from the normalization, background, neutron time of flight, sample thickness, and temperature. All these uncertainties were included in the evaluation process.

The ^{103}Rh resonance parameter and RPC derived in this work were converted into the ENDF format using LRF = 7 for the resonance parameters and LCOMP = 2 for the covariance. As mentioned previously, LRF = 7 allowed for the use of the spin channel feature that was not captured in a previous ^{103}Rh resonance evaluation. LCOMP = 2, also known as a compact format, was used for covariance representation to save computer storage.

The original ENDF format option for covariance storage is LCOMP = 1. Although the results of calculations with LCOMP = 1 were equivalent to LCOMP = 2, LCOMP = 1 led to a covariance data storage size that was eight times larger than that of LCOMP = 2. The prescription developed for LCOMP = 2 consisted of mapping the actual correlations into numbers in between -1 and $+1$ and dropping values that were between $-10^{-NDIGIT}$ and

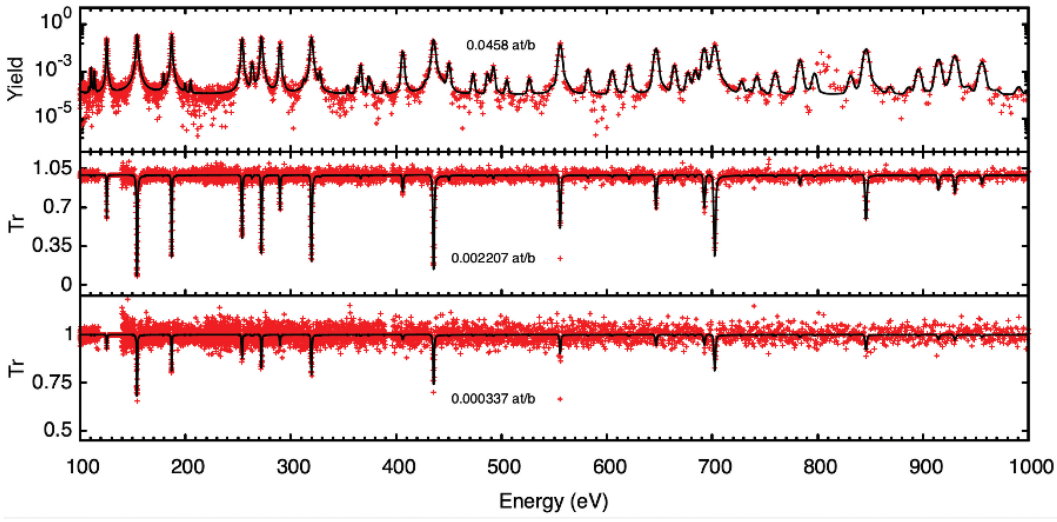

Fig. 15. SAMMY fitting of the transmission and yield data of Brusegan et al.[16]

TABLE IX

Average Level Spacing and Neutron Strength Function*

J^{π}	<D>	$10^{4} \times S_{nl}$
0^{-}	109.99 (3269)	0.096 (8)
1^{-}	39.32 (608)	0.14 (8)

*Average level space in electron-volts.

TABLE X

Missing Level Estimation

Energy Range (eV)	Percentage of Missing Resonances (%)
0 to 500	0.8
0 to 1000	6.75
0 to 4000	22.27
0 to 8000	38.54

$+10^{-NDIGIT}$, where *NDIGIT* is an integer in which the allowed values were from 2 to 6. The smaller the *NDIGIT*, the less storage was required.

Three digits were needed to reproduce the uncertainty calculated by SAMMY with a stable covariance matrix and no negative eigenvalues. The ENDF-formatted covariance library was processed using the PUFF module of the AMPX[26] for a flat neutron spectrum and a 44–neutron energy group. The results for the capture cross section are displayed in Fig. 18, which was generated by the NJOY code.[27]

The covariance above 8000 eV was that in the ^{103}Rh ENDF/B-VIII.0 evaluation.

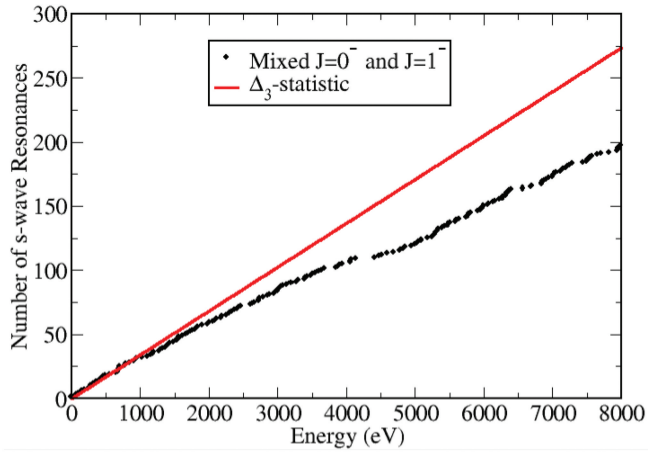

Fig. 16. Cumulative number of resonances up to 8000 eV.

IV. BENCHMARK RESULTS

The performance of the ^{103}Rh resonance evaluation generated in this work was investigated for benchmark systems sensitive to ^{103}Rh. In addition to the results using ENDF/B-VIII.0 as the base library, calculations using the JEFF3.3[20] library were also performed. The cross-section libraries used in the calculations included the new resolved resonance evaluation developed in this work and a recent unresolved resonance evaluation.[28] The testing libraries were generated by replacing the ^{103}Rh resolved and unresolved resonance evaluations of the ENDF/B-VIII.0 and JEFF3.3 libraries with the new evaluations. The testing libraries are referred to as ENDF/B-VIII.0 + RR + URR and JEFF3.3 + RR + URR, respectively. Very few critical benchmark systems sensitive to

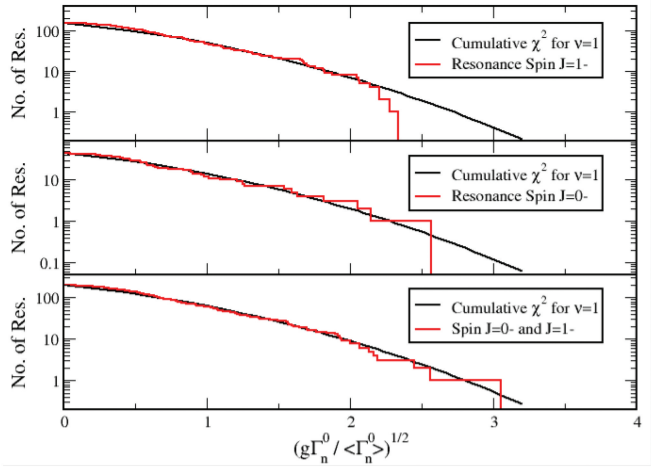

Fig. 17. Cumulative Porter-Thomas *s*-wave resonances.

the ^{103}Rh cross sections are available in the literature,[29] and those that are available all exhibited a sensitivity in the thermal energy spectrum.

The Institute for Radiological Protection and Nuclear Safety (IRSN, from the French name Institut de Radioprotection et de Sûreté Nucléaire) participated in critical experiments aimed at nuclear data measurements for code and data validations, in particular for testing the ^{103}Rh cross-section data and uncertainties. The critical benchmark program, named Matériaux Interaction Réflexion Toutes Epaisseurs (MIRTE), was designed by IRSN and carried out at the CEA (Commissariat à l'Energie Atomique) Valduc Center in the Apparatus B assembly.

In particular, the benchmark listed in the International Criticality Safety Benchmark Evaluation

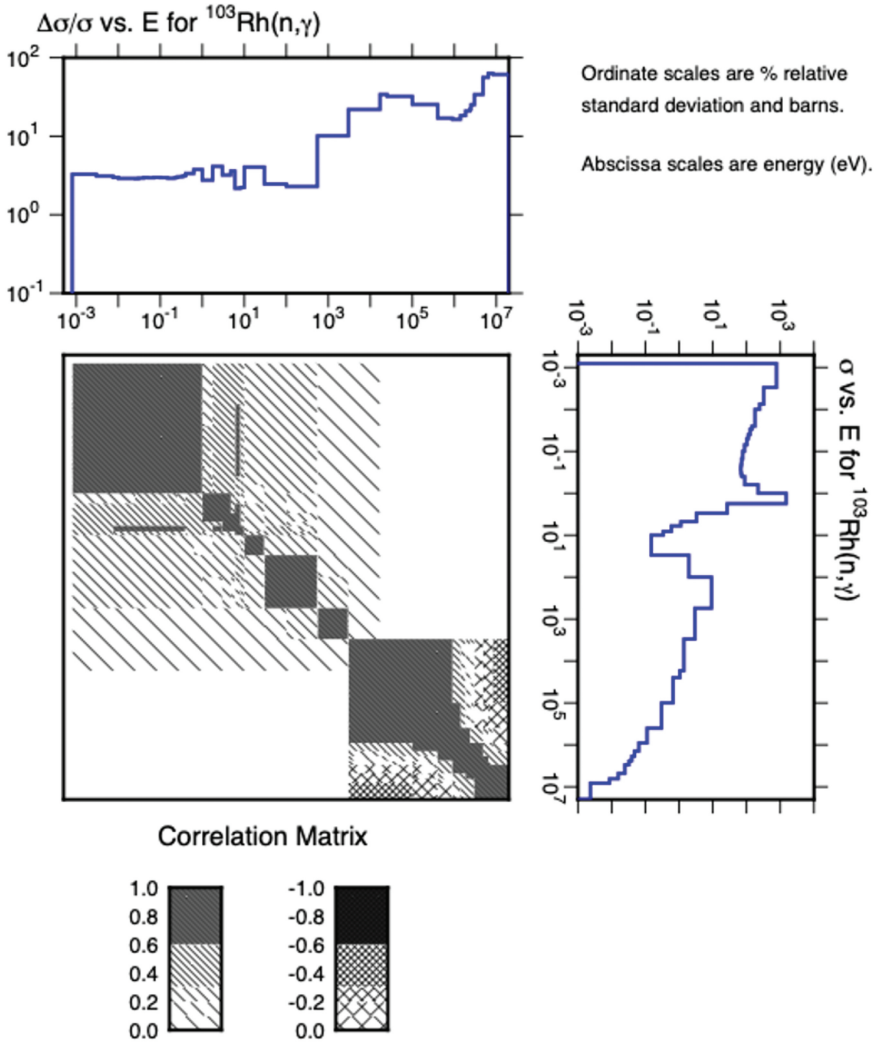

Fig. 18. Uncertainty and correlation for the ^{103}Rh capture cross section.

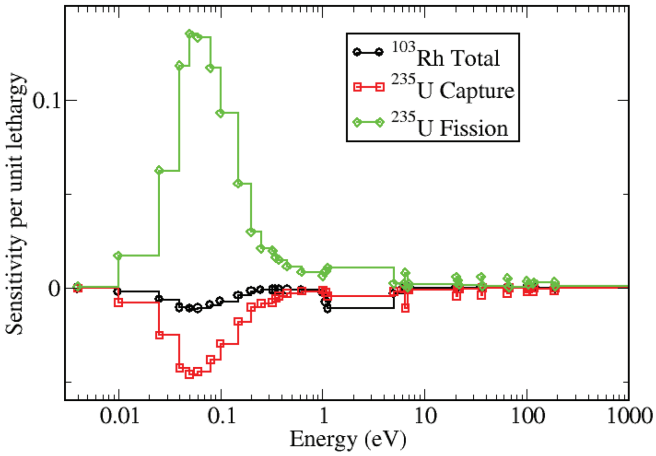

Fig. 19. k_{eff} sensitivities to ^{103}Rh and ^{235}U for the LEU-COMP-THERM-106 benchmark cross sections.

Project handbook,[29] identified as LEU-COMP-THERM-106, was designed to be sensitive to ^{103}Rh capture.[30] The sensitivity of k_{eff} to the ^{103}Rh total cross section (quite similar to capture in the thermal energy range) is shown in Fig. 19. Also shown in Fig. 19 are the sensitivities of k_{eff} to the capture cross section of ^{235}U and the fission cross section of ^{235}U. The sensitivities were generated based on the JEFF3.3 library with the MORET code[31] for energy bin boundaries corresponding to the SCALE 56-group structure.[32] The prior uncertainty owing to the ^{103}Rh data was determined using the sensitivities produced by the MORET code and the covariance matrix generated with the NJOY processing tool[27] in the MACSENS GLLSM tool.[33]

Cross-section libraries in the ACE (a compact ENDF) format were generated with the NJOY code, and k_{eff} was calculated using the MORET code and a statistical uncertainty of about 20 pcm (1 pcm = 0.00001 Δk). The results are displayed in Table XI.

Comparisons of the ENDF/B-VIII.0 results with calculations using the ENDF/B-VIII.0 + RR + URR library indicated a decrease in Δk corresponding to about 80 pcm, whereas for the JEFF3.3 and JEFF3.3 + RR + URR libraries, the decrease in Δk was about 50 pcm. The uncertainty owing to the total cross section of ^{103}Rh was calculated by the MACSENS code as 128 pcm. This value was consistent with the difference observed between the benchmark k_{eff} and the calculated values.

TABLE XI

Comparisons of k_{eff} Results

Evaluation	k_{eff} Results
Benchmark	1.00040 (64)
JEFF3.3	1.00213 (20)
JEFF3.3 + RR + URR	1.00163 (20)
ENDF/B-VIII.0	1.00296 (21)
ENDF/B-VIII.0 + RR + URR	1.00216 (22)

The result with the new evaluation was within the benchmark experimental uncertainties at the 2σ level, showing good consistency with the benchmark k_{eff} and showing an improvement compared with other evaluations of nuclear data. Overall, the new evaluation provided a good indication that the criticality safety prediction for thermal systems containing ^{103}Rh has improved. Furthermore, the covariance and uncertainties generated were consistent with the integral benchmark uncertainties.

V. CONCLUSION

The resolved resonance evaluation of the ^{103}Rh cross sections included several experimental data sets, with an emphasis on new capture measurements. Issues with resonance representations present in previous evaluations were addressed. The use of high-resolution experimental data extended the resonance evaluation energy range from 4000 to 8000 eV. RPC and uncertainties were also generated. Information, such as coherent and incoherent scattering, thermal cross-section values, Westcott factors, and resonance integrals, was added to the evaluation process.

A thorough statistical analysis of the resonance parameters provided an adequate estimate of the number of missing resonances. Although many resonances were not resolved, the SAMMY fit of the experimental data was not affected. The thermal benchmark results indicated that the new ^{103}Rh resolved resonance evaluation was as good as those of existing evaluations or even potentially slightly better. Presently, no benchmark in the epithermal energy region exists to test the efficiency of the new evaluation.

Acknowledgments

This paper has been authored by UTBattelle, LLC, under contract DEAC0500OR22725 with the U.S. Department of Energy (DOE). The U.S. government retains and the publisher, by accepting this paper for publication, acknowledges that the U.S. government retains a nonexclusive, paid-up, irrevocable, worldwide license to publish or reproduce the published form of this paper, or allow others to do so, for U.S. government purposes. DOE will provide public access to these results of federally sponsored research in accordance with the DOE Public Access Plan (https://www.energy.gov/doe-public-access-plan).

Funding

This work was supported by the Nuclear Criticality Safety Program, funded and managed by the National Nuclear Security Administration for the DOE. Part of this work was carried out when the first author, Luiz Leal, was at the IRSN. Additionally, this work is part of an action sheet under the EURATOM/DOE agreement.

Disclosure Statement

No potential conflict of interest was reported by the authors.

ORCID

Luiz Leal http://orcid.org/0000-0002-7488-0667

References

1. I. C. GAULD, G. ILAS, and G. RADULESCU, "Uncertainties in Predicted Isotopic Compositions for High Burnup PWR Spent Nuclear Fuel," NUREG/CR-7012/ORNL/TM-2010-10/41, U.S. Nuclear Regulatory Commission/Oak Ridge National Laboratory (2011).
2. N. M. LARSON, "Updated Users Guide for SAMMY: Multi-Level R-Matrix Fits to Neutron Data Using Bayes' Equations," ENDF-364/R2, Oak Ridge National Laboratory (2008).
3. D. A. BROWN et al., "ENDF/B-VIII.0: The 8th Major Release of the Nuclear Reaction Data Library with CIELO-project Cross Sections, New Standards and Thermal Scattering Data," *Nucl. Data Sheets*, **148**, 1 (2018).
4. M. HERMAN and A. TRKOV, "ENDF-6 Formats Manual, Formats and Procedures for the Evaluated Nuclear Data Files ENDF/B-VI and ENDF/B-VII," Report- BNL-90365-2009 Rev. 1, National Nuclear Data Center, Upton, New York (2010).
5. N. OTUKA et al., "Towards a More Complete and Accurate Experimental Nuclear Reaction Data Library (EXFOR): International Collaboration Between Nuclear Reaction Data Centres (NRDC)," *Nucl. Data Sheets*, **120**, 272 (2014); https://doi.org/10.1016/j.nds.2014.07.065.
6. A. BRUSEGAN and J. M. SALOME, "GELINA: A Modern Accelerator for High Resolution Neutron Time of Flight Experiments," *Nucl. Instrum. Methods*, **155**, 11 (1978); https://doi.org/10.1016/0029-554X(78)90181-7.
7. E. R. GAERTTNER, M. L. YEATER, and R. R. FULLWOOD, "Rensselaer Polytechnic Institute LINAC Facility," presented at the Symp. on Neutron Physics, Rensselaer Polytechnic Institute, May 1961.
8. D. BARRY, Naval Nuclear Laboratory, Schenectady, New York, Personal Communication 2016.
9. L. LEAL et al., "Testing of a New ^{103}Rh Resolved Resonance Evaluation," presented at the 2021 ANS Winter Mtg. and Technology Expo, Washington D.C., November 30–December 3, 2021.
10. L. C. MIHAILESCU et al., "Neutron Cross-Section Measurements on ^{103}Rh and ^{133}Cs for Improved Nuclear Criticality Safety," *NEMEA-3 Neutron Measurements, Evaluations and Applications, Proceedings of the Enlargement Workshop*, A. J. M. PLOMPEN, Ed., Borovets, Bulgaria, October 25–28, 2006 (2006).
11. R. O. SAYER, "Updated Users' Guide for RSAP—A Code for Display and Manipulation of Neutron Cross Section Data and SAMMY Fit Results," ORNL/TM-2003/133, Oak Ridge National Laboratory (July 2003).
12. L. C. LEAL et al., "R-Matrix Analysis of ^{235}U Neutron Transmission and Cross-Section Measurements in the 0- to 2.25-keV Energy Range," *Nucl. Sci. Eng.*, **131**, 230 (1999); https://doi.org/10.13182/NSE99-A2031.
13. F. H. FRÖHNER and O. BOULAND, "Treatment of External Levels in Neutron Resonance Fitting: Application to the Nonfissile Nuclide ^{52}Cr," *Nucl. Sci. Eng.*, **137**, 70 (2001); https://doi.org/10.13182/NSE01-A2176.
14. P. RIBON, "Études de quelques propriétés des niveaux excites des noyaux composes formes par !'interaction des neutrons lents avec 103Rh, Xe, 155Gd, 232Th," Thesis, CNRS, A.0.3560 (1969), also CEA Note N-1149 (1969).
15. S. LEE et al., "Neutron Capture Cross-Section Measurement of Rhodium in the Energy Region from 0.003 eV to 80 keV by Linac Time-of-Flight Method," *Nucl. Sci. Eng.*, **144**, 94 (2003); https://doi.org/10.13182/NSE03-A2345.
16. A. BRUSEGAN et al., "Neutron Capture and Transmission Measurements on ^{103}Rh Down to Thermal Energies," *Proc. Int. Conf. Nuclear Data for Science and Technology*, Santa Fe, New Mexico, September 26–October 1, 2004.
17. W. W. HAVENS JR and J. RAINWATER, "The Slow Neutron Cross Sections of Indium, Gold, Silver, Antimony, Lithium, and Mercury as Measured with a Neutron Beam Spectrometer," *Phys. Rev.*, **70**, 154 (1946); https://doi.org/10.1103/PhysRev.70.154.
18. V. L. SAILOR, "The Parameters for the Slow Neutron Resonance in Rhodium," *Phys. Rev.*, **91**, *1*, 53 (1953); https://doi.org/10.1103/PhysRev.91.53.
19. "Evaluation of Measurement Data—Guide to the Expression of Uncertainty in Measurement," JCGM 100:2008 (2008); https://www.bipm.org/documents/20126/

2071204/JCGM_100_2008_E.pdf/cb0ef43f-baa5-11cf-3f85-4dcd86f77bd6 (current as of Sep. 21, 2024).

20. A. J. M. PLOMPEN et al., "The Joint Evaluated Fission and Fusion Nuclear Data Library, JEFF-3.3," *Eur. Phys. J. A*, **56**, 181 (2020).
21. S. F. MUGHABGHAB, *Atlas of Neutron Resonances Resonance Parameters and Thermal Cross Section Z=1–100*, Elsevier, Amsterdam (2006). See also B. PRITYCHENKO and S. F. MUGHABGHAB, "Neutron Thermal Cross Sections, Westcott Factors, Resonance Integrals, Maxwellian Averaged Cross Sections and Astrophysical Reaction Rates Calculated from Major Evaluated Data Libraries," *Nucl. Data Sheets*, **113**, 3120.
22. L. LEAL et al., "Resonance Parameter and Covariance Evaluation for ^{16}O up to 6 MeV," *EPJ Nucl. Sci. Technol.*, **2**, 43 (2016); https://doi.org/10.1051/epjn/2016036.
23. F. FERNANDEZ-ALONSO and D. L. PRICE, "Neutron Scattering – Fundamentals," *Volume 44, "Appendix – Neutron Scattering Lengths and Cross Sections," pages 471–528*, Academic Press (2013).
24. S.-Y. OH, J. CHANG, and L. C. LEAL, "Statistical Assignment of Neutron Orbital Angular Momentum to a Resonance," *Nucl. Sci. Eng.*, **148**, 43 (2004); https://doi.org/10.13182/NSE04-A2439.
25. L. C. LEAL and N. M. LARSON, "SAMDIST: A Computer Code for Calculating Statistical Distributions for R-Matrix Resonance Parameters," ORNL/TM-13092, Oak Ridge National Laboratory (1995).
26. D. WIARDA et al., "AMPX-6: A Modular Code System for Processing ENDF/B," ORNL/TM-2016/43, Oak Ridge National Laboratory (2016).
27. R. MACFARLANE et al., "The NJOY Nuclear Data Processing System, Version 2016," LA-UR-17-20093, Los Alamos National Laboratory (Jan. 2017).
28. D. P. BARRY et al., "A New ^{103}Rh Unresolved Resonance Region Evaluation," *Ann. Nucl. Energy*, **188**, 109751 (2023); https://doi.org/10.1016/j.anucene.2023.109751.
29. N. LECLAIRE et al., "International Handbook of Evaluated Criticality Safety Benchmark Experiments," NEA/NSC/DOC (95)/03, Organisation for Economic Co-operation and Development/Nuclear Energy Agency (2021).
30. N. LECLAIRE et al., "The MIRTE Experimental Program: An Opportunity to Test Structural Materials in Various Configurations in Thermal Energy Spectrum," *Nucl. Sci. Eng.*, **178**, *4*, 1 (2014); https://doi.org/10.13182/NSE14-29.
31. A. JINAPHANH, N. LECLAIRE, and B. COCHET, "Continuous-Energy Sensitivity Coefficients in the MORET Code," *Nucl. Sci. Eng.*, **184**, *1*, 53 (2016); https://doi.org/10.13182/NSE16-2.
32. B. T. REARDEN and M. A. JESSEE, "SCALE Code System," ORNL/TM-2005/39 Version 6.2.1, Oak Ridge National Laboratory (Aug. 2016).
33. F. FERNEX and N. LECLAIRE, "A New IRSN Tool for Nuclear Data Bias Assessment: MACSENS V3.0 GLLSM Module," *Proc. Nuclear Criticality Safety Division Topl. Mtg.* (*NCSD 2022*), pp. 256–264, Anaheim, California, June 12–16, 2022 (2022).